Microphotonics for monitoring the supramolecular thermoresponsive behavior of fatty acid surfactant solutions

R. Castro-Beltrán, Lucas Garnier, A. Saint-Jalmes, Hervé Lhermite, H. Cormerais, Anne-Laure Fameau, Eric Gicquel, Bruno Bêche

Microphotonics for monitoring the supramolecular thermoresponsive behavior of fatty acid surfactant solutions

R. Castro-Beltrán[a], L. Garnier[b], A. Saint-Jalmes[b], H. Lhermite[c], H. Cormerais[c,d], A.-L. Fameau[e], E. Gicquel[b], B. Bêche[b,c]

[a] *Universidad de Guanajuato, Departamento de Ingeniería Física, División de Ciencias e Ingenierías-León, Guanajuato, México*
[b] *Univ Rennes, CNRS, IPR (Institut de Physique de Rennes) - UMR 6251, F-35000 Rennes, France*
[c] *Univ Rennes, CNRS, IETR (Institut d'Electronique et de Télécommunicationde Rennes)- UMR 6164, F-35000 Rennes, France*
[d] *Centrale/Supelec, Campus de Rennes, 35510 Cesson-Sévigné, France*
[e] *INRA-BIA, Biopolymères Interactions Assemblages, 44316 Nantes, France*

E-mails: lucas.garnier@univ-rennes1.fr and bruno.beche@univ-rennes1.fr

Abstract

The development and the ability of an optical integrated polymeric resonator, acting as a surface light probe, for monitoring temperature-induced supramolecular phase transitions is presented in this work. The homogeneous detection of the transitions between different self-assembled structures in an aqueous solution of fatty acids (12-hydroxystearic acid, in association with amino-pentanol) was studied by investigating the coupling between the solution and the integrated photonic micro-cavity. Tuning the self-organized assemblies of surfactant is very attractive for many applications, such as cosmetic products, food, drug delivery and medical, and the development of alternative tools - especially those requiring minute amount of solution - to monitor their structural changes are essential. These original studies at temperatures ranging from 17 to 24 °C, based on a statistical treatment of optical resonance spectra, have evidenced the thermoresponsive nature of the optical features, and that different regimes occur with temperature. The optical results were corroborated with the measurement of the solution viscosity as a function of temperature, confirming that we can ascribe the optically-detected regimes to a surfactant assembly shifting reversibly from a tubular shape to a micellar one. The comparison between the optical and the rheological responses showed different accuracies: while the viscosity data exhibited a rather smooth and monotonous transition, the behavior changes were sharper and non-monotonous in terms of optical properties, allowing us to unambiguously identify in intermediate regime between 18.5 and 20°C. These morphological transition experiments represent a unique opportunity to extend the numbers of available techniques studying these systems through integrated optical techniques with potential opportunities of real time detection and working on low sampling volume.

Keywords: Micro-technologies, polymers, photonics, fatty acid, thermos-responsive surfactant system

1. Introduction

A micro-encapsulation process is a useful procedure for packing, isolation and protection of biochemical compounds, and self-assembled supramolecular structures - such as micelles, vesicles or lamellar phases - represent an extraordinary opportunity for encapsulation. A structure that could be filled by bio-chemical compounds is a potential prospect for drug delivery in medicine, environment science, cosmetics and food transformation [1-3]. These applications depend on the complete control of the intrinsic self-assembled supramolecular structures, linked to a reorganization at the molecular scale [4-6]. From the vast family of lipids, fatty acids are predominant and very important for a huge number of biotechnological applications ranging from sources of fuel for animals, cosmetic products to drug delivery carriers [2, 3, 7]. These systems can be modulated in various shapes adapted to the use of fluids and gels or creams and pastes. From these derivative applications, their supramolecular tunable and reversible structures are highly related to their bulk properties such as viscosity and thermal behavior.

There are numerous techniques for investigating supramolecular arrangements, like Differential Scanning Calorimetry (DSC), various microscopies, Wide-Angle X-ray Scattering (WAXS), Small-Angle Neutron Scattering (SANS), or rheometry. Those are some of the used technological tests to characterize the morphological and mechanical properties of many self-assembled structures and their different phases [6, 8]. These techniques play complementary roles by providing information at different length and time scales. Various bulk and surface optical techniques, based on scattering intensity modulation, have been proposed to detect the phase transition temperatures of products in biology [9]. Looking for another sensitive techniques that present an opportunity for monitoring fine-changes associated to phase transition, microresonators [10, 11] based on integrated optical (IO) chip devices and resonant probe light are shown as outstanding photonic platforms for this type of biochemical sensing applications [12-15]. The sensing mechanisms that define the biochemical performance of optical resonators can be classified as surface- and homogeneous-sensing. The first is related to the capability of the resonator to identify a specific analyte through previous surface functionalization protocols [12-13]. On the other hand, in the second one, any cladding variation induces a change that can be detected by the resonator over the background signal. This cladding variation will induce a change in the effective refractive index n_{eff} [12, 13, 16, 17]. For the scope of this work, we will focused on the second sensing mechanism: the homogeneous sensing. Regardless the involved sensing schemes, the shift of the resonant spectrum should be temperature independent which implies that the design of the microresonator based on waveguide be quasi-athermal; a low dependence of temperature on optical properties is mandatory in this IO chip to ensure stability and

to avoid misunderstanding in the interpretation of the output signal [15]. The thermo-optical effect of a material obviously does not exhibit symmetry breaking or slope reversal in its behavior as a function of a temperature ramp; it is characteristic of a monotonous function as measure in the following.

To demonstrate the viability of IO chip, based on a laterally coupled racetrack microresonator, as an alternative technique to monitor temperature-induced phase transitions, we selected a chemical system, belonging to the family of fatty acids with both bio-degrability and low toxicity, under their deprotonated forms. Such fatty acid molecules can self-assemble under various shapes in an aqueous solution. These self-assembled structures can respond to stimuli such as pH, presence of CO_2 and temperature, due to changes occurring at the molecular level [19]. In this group of fatty acids, the 12-hydroxystearic acid (named 12-HSA in the following) is remarkable as it can provide - once associated with alkanolamine counterions - thermo-responsive supramolecular structures [4-6]. At low temperature, self-assembled multilayer tubes (with typical length of tens of µm, and diameter of a few µm) are found due to the ion pairing of 12-HSA with an alkanolamine. Above a critical temperature, such tubes vanish and only nanometric micelles are detected. The transition temperature depends on the relative ratio of the 12-HSA and of the counterion, and on the choice of alkanolamine ; it can then be adjusted from 18°C to 70°C. Therefore, drastic structural transitions at the supramolecular scale are found with this chemical system when temperature is changed, providing us with an ideal candidate to test the IO chip.

2. Materials and Methods

2.1 IO device based on polymeric microresonator

The resonant quantifications met in such physical systems are due to a geometric recirculation of the light. These quantifications emerge thanks to the installation of a cyclic condition (or stationary waves) written as $P_{opt}=m.\lambda_{Maxwell}$, with P_{opt} the 'optical'-perimeter of the microresonator and m an integer. This principle can also be seen as the quantification of the orbital kinetic momentum $\vec{L}$ as a quantified photonic orbit. Integrated polymeric microresonators are fabricated through deep UV (DUV) photolithography procedures and are based on UV210 photoresist. A key point refers to the use of this specific photoresist chemistry product, hinging on deep UV light/matter interactions [20]. UV210 compound is a polymer responsive to shorter exposure wavelengths when compared to with the standard procedures normally using conventional *i*-line from a mercury lamp. This specific DUV-polymer is made of poly p-hydroxystyrene and poly t-butyl acrylate; it is called an amplified

chemical photoresist including a photo acid generator so as to increase the sensitivity with energy exposure and to obtain a better photolithography mechanism. It is well reported that this process has allowed resolutions <400nm in the size of the IO devices. The whole fabrication procedure and the full quality control of the photonic device is reported elsewhere [21, 22]. The microresonator is based on a racetrack shape and light is laterally coupled with a straight tapered optical waveguide, Figure 1. A tapered bus optical waveguide ensures single mode operation of the IO micro-device. In comparison with other microcavities, a racetrack shape presents some advantages linked to its elongated rib zone (define by the coupling length, L_c). This length L_c, the parallelism between this resonator and the tapered rib waveguide, contribute to a stronger optical coupling strength of the microresonator [23]. A length L_c= 5 µm, a radius R= 5 µm, a width w= 3 µm and a gap g= 400 nm (a distance from the tapered waveguide and the microcavity) represent the main geometrical features of our micro-racetrack. The small size of these specific resonators makes possible to take strongly localized measurements spatially with very low volume of products.

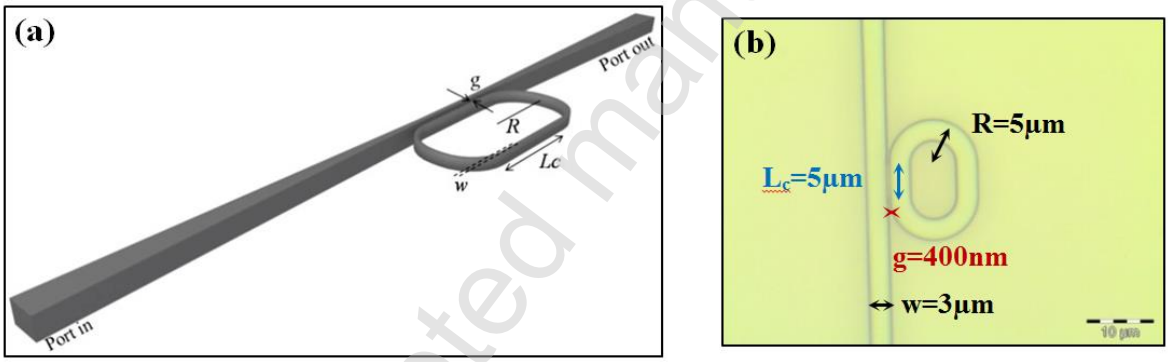

Fig. 1. (a) Sketch of the racetrack polymer resonator. (b) Top view photograph (x20) of the racetrack with$R$, L_c, w and g are the main geometrical parameter define the IO micro-device.

Since the resonator consists of a straight guide portion of UV210 (n_{UV210} close to 1.60 at a λ_0=795 nm wavelength) plus another curved guide (radius of curvature R = 5 µm), it is possible to estimate and therefore predict the single-mode behavior by finite difference method as explained in ref. [24]. Figure 2 represents the simulations implemented by a semi-vectorial finite difference method, respectively the eigenvalues of the effective indices $n_{eff}^{phase} = \frac{\beta.\lambda_0}{2\pi}$ (β representing the effective propagation constant), plus the associated TE_{00} single-mode (eigenvector or optical mode distribution) into such an overall structure.

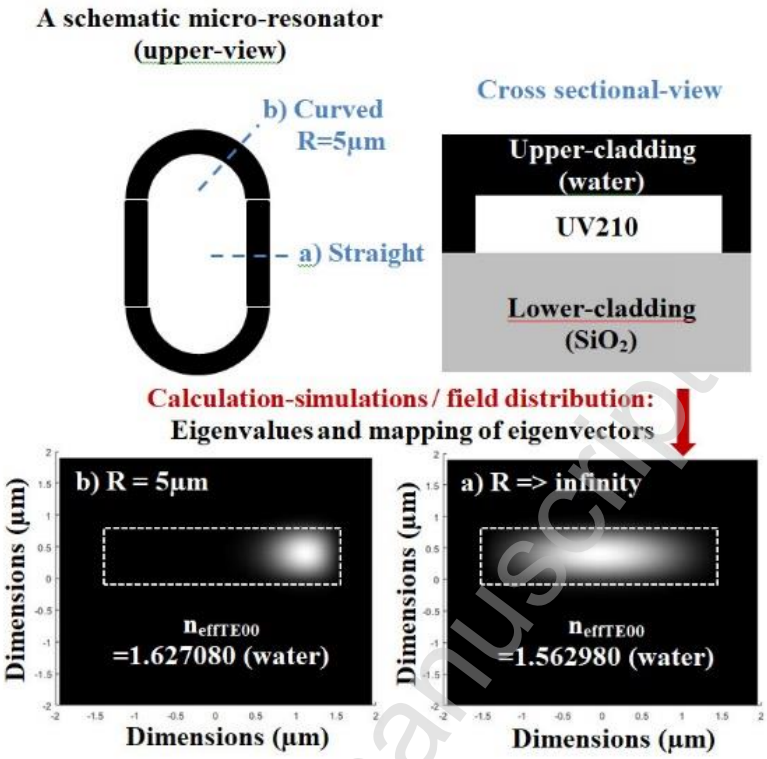

Fig. 2. Schematic diagram of the MRs structures (upper and cross-sectional views); eigenvalues and mapping of eigenvectors (field magnitude and distribution explained in ref. [24]) simulations by semi-vectorial finite difference method (n_{UV210}=1.60 and n_{SiO2}=1.45 at λ_0=795nm, *R*-curved radius, waveguide thickness and width of 5 µm, 0.9µm and 3 µm respectively); the upper cladding corresponds in these simulations to the water liquid which present index value of 1.33. In the two regions concerned of the resonator element (straight and curved) the optical mode corresponds to a guided mode of the light cone.

This spatial semi-vectorial finite difference method is associated to a Conformal Transformation (CT) of the complex plane, which allow to consider the curved guide as an effective straight guide with a modified profile of index [25, 26]. These modelisations confirm that the curved part of the resonator still guide the light despite the lateral shift of the eigenmode clearly visible on Figure 2 (b). This is strongly accentuated by these structures with low radius of curvature R = 5 µm, with w = 3 µm. Indeed, such R provokes via the CT an effective augmentation of the index of $\Delta n = \frac{n_{DUV210}}{2}\frac{w}{R} \approx 0.48$ [25, 26]. The eigenmode stays a guided mode of the light cone, as shown by the experiments in the following. In order to perform these simulations, the upper cladding was considered water.

These previous simulations confirm the single-mode behavior of such opto-geometric resonant microstructures. The experiments will be conducted with a broad-spectrum source (>40nm), so the light will feel the total index n_{total} of the whole structure which takes into account the modal dispersion. A first order expansion of Taylor-Lagrange is sufficient to properly describe the modal dispersion that can be written $n_{eff}^{total}(\lambda) = n_{eff}^{group}(\lambda_0) + \lambda.\left[\frac{\partial n_{eff}^{phase}}{\partial \lambda}(\lambda_0)\right]$, with $n_{eff}^{group}(\lambda_0) = n_{eff}^{phase}(\lambda_0) - \lambda_0\left[\frac{\partial n_{eff}^{phase}}{\partial \lambda}(\lambda_0)\right]$ [27]. The total index is clearly higher than the effective phase index and can reach 1.9 because two dispersive contributions are simultaneously added: at first, the physical dispersion of the materials (including the one of the UV210 organic which is strong in the intense red radiation) plus the modal dispersion contribution which is specific to the mathematical non-linearities of the dispersion curves of such guiding and resonant structures. Thus, it is this total index that must be taken into account in the resonance parameters of the structures (Free Spectral Range FSR, finesse) that will be probed by the broad-spectrum source of light [27]. The FSR is defined as the spectral distance between two wavelengths which resonate FSR=$\frac{(\lambda_0)^2}{P.n_{eff}^{tot}}$, with *P* the racetrack perimeter and λ_0 the central wavelength of the broadband source. The FWHM, which is defined as the Full Width at Half Maximum of a resonance peak obeys to $FWHM = \frac{\lambda_0^2}{\pi P n_{eff}^{tot}}\ arccos\left(\frac{2AK}{1+A^2K^2}\right) = \frac{FSR}{\pi} arccos(\frac{2AK}{1+A^2K^2})$ with K related to the coupling and A to the loss both in the coupling zone and during the circulation inside the resonator. In conclusion, by considering these geometrical conditions, the global optical group index of the system at $\lambda_0 = 800$ nm with 40 nm of broadband, we can ensure that the IO device is operating exclusively in the single optical modes.

2.2 Optical characterization

The experimental protocol is based on the sketch of Figure 3. The IO micro-racetrack is optically pumped with a laser source (SLD 331 HP3) centered at $\lambda_0 = 800$ nm with 40 nm of broadband while the detection is based on an integral protocol relying on a dual visualization of the micro-device and its electromagnetic mode (TE_{00}-TM_{00}); furthermore, a permanent capture of the best optical transmission properties by both an optical power-meter and an optical spectrum analyzer (OSA-Ando AQ-6315E) are carried out.

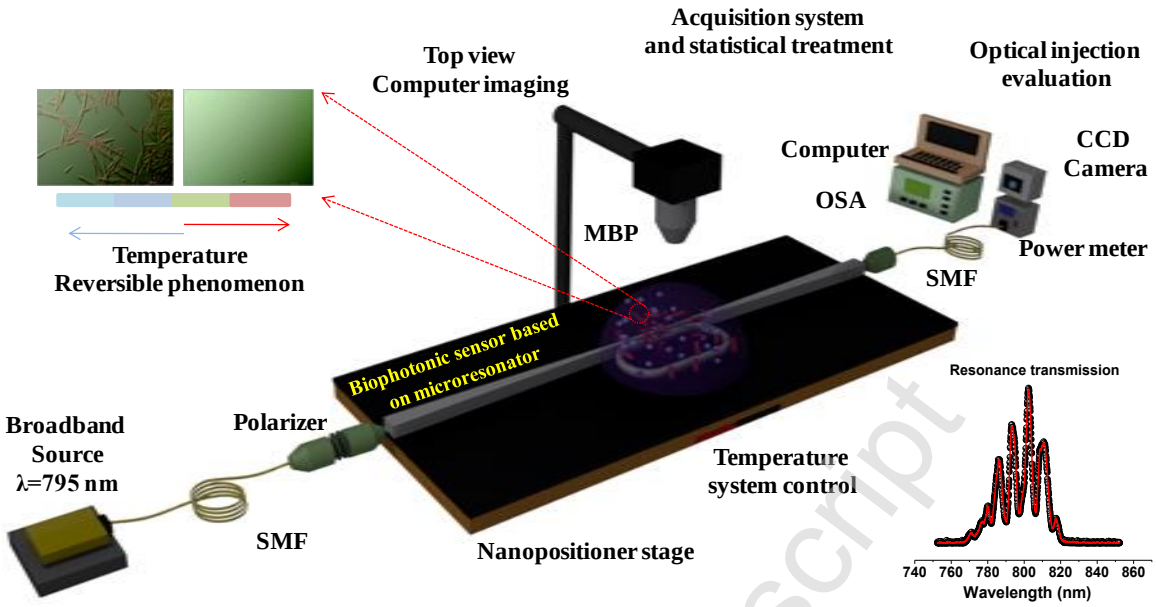

Fig. 3. Experimental setup for the full optical characterization of the microcavities and the complete fatty acid phase-transition monitoring protocol. The relative positions of microscope objectives and the device are controlled by piezoelectric nanopositioners. The temperature of the integrated photonic chip is controlled by a thermostatic mount on which the micro-chip rests. All data from OSA is automatically recorded by computer and statistically analyzed and presented.

Respectively, a top view of the microcavity (full visualization of the confinement of light traveling along the device) and a cross-sectional view of the single mode propagation are recorded by a micro beam profile (MBP) system and an IR-camera. The best coupling configuration is achieved once both a maximum optical intensity from a power-meter and a well defined single-mode are observed. The inset in Fig. 3 shows the typical resonance spectrum, highlighting the main optical parameter on the graph: among these, the Free Spectral Range (FSR) which represents the periodicity of the quantized spectrum or the spectral distance between two wavelengths which plus the Full Width at Half Maximum (FWHM) that is related to the finesse of the color or the light chord. The quality factor (Q) of the device can also be extracted from the spectra. These spectral parameters will evolve during the transition. Microscope objectives are used for both the injection and the collection of the light, and are mounted on piezoelectric nano-positioners for optimal injection conditions. The photonic chip is mounted on a Peltier temperature controller in order to investigate the behavior of the fatty acid solution with temperature. A drop of a few µL of the hybrid C5 (5-amino-1-pentanol) plus 12-HSA (12-hydroxystearic acid) solution is deposited on the surface of the sensor using a µL pipette. An optical spectrum analyzer connected to a computer acquires the output signal of the resonator. The measurements are performed as a function of temperature on the range [17-24]°C, with a step of 0.5°C. For each temperature, 10 spectra are

collected in order to reduce the error on the measurements. Figure 4 represents a typical resonant spectrum.

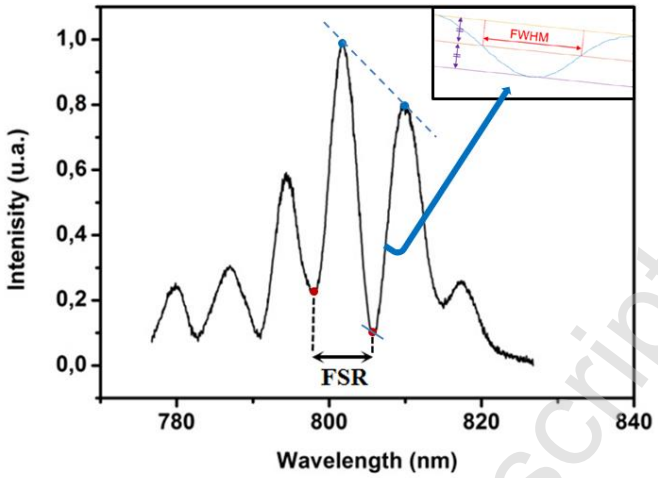

Fig. 4. Typical resonant spectrum at fixed temperature of the photonic device detected and stored by OSA and computer; the FSR is close to 8 nm in agreement with the opto-geometrical structure. Inset represents the synoptic of the method for the FWHM calculus of the comb-shaped periodic wavelength.

The pseudo-period or Free Spectral Range (FSR) is calculated by a classical Fast Fourier Transform (FFT) of the resonant spectrum or comb-shaped periodic wavelength and also corroborated by a numerical derivation to localize all the extrema. Then, the Full Width at Half Maximum (FWHM), synoptic of the method described into inset, is also extracted from the raw spectra by our own Matlab computational code; such a code can be installed into an embedded system (Raspberry Pi…). The latter was developed respectively to control the remote spectrum analyzer and record the spectra, then to calculate the FSR and FWHM parameters by a specific signal processing code. Calculations and signal processing are performed at each spectrum acquisition in order to extract and to plot the FSR(T), FWHM(T) and Q(T) parameters over temperature T.

2.3 Sample preparation

As already pointed out, the 12-hydroxystearic acid (12-HSA) can be associated to different alkanolamines, and at different relative concentrations to set the transition temperature. Here, we selected experimental conditions leading to a transition close to the room temperature. This corresponds to the selection of the 5-amino-1-pentanol (C5) in the alkanolamine group, and to a molar ratio R=0,3 (as defined in [6]). In practice, 12-HSA and C5 are weighted and added to ultra-pure water, in order to reach the ratio R=0.3. The mixture was then heated at 80°C to insure a complete dispersion

3. Results and discussion

As the type of the supramolecular phases of the hybrid C5/12-HSA compound depends on temperature, it is required that the thermal features of the chip-device allow to monitor these changes. From previous studies focused on the detection of gel/fluid phase transition of biological compounds using polymeric microcavity, an extended experimental and computing protocol were presented in ref. [16]. On such devices, the thermal dependences of the main optical properties at the Si/SiO_2/UV210/air configuration were presented, and it was concluded that the thermo-optical properties of the IO microresonator based on UV210 polymer have a high quality, verifying its high thermal stability [16].

3.1 The hybrid C5 /12-HSA supramolecular structures and the effect of temperature

The phase diagram of the C5/12-HSA compound shows a large supramolecular polymorphism, with structures ranging from long cylindrical tubes to spherical micelles (Figure 5). The figures 5(a) and (b) show the morphologies of the C5/12-HSA supramolecular structures obtained at a temperature T= 7.5°C. The structure of the 12-HSA/alkanolamine, at low temperatures, has been widely studied by various techniques (neutron and X-Ray scattering) and has highlighted that the 12-HSA molecules self-assemble into multi-lamellar tubes [4-6]. The images Fig. 5(a) and (b) were taken by using an optical microscope in its phase contrast mode and by TEM respectively. For the optical microscopy, the samples were directly deposited on a wafer at a specific temperature: once all water has evaporated the phase contrast micrographs were captured. At low T, by studying the distribution and the statistic histograms, long tubular structures are shown with length equal to 32.8±16.8 µm and width of 2.1±1.1 µm. On the other hand, once temperature is above a critical value, the liquid turns transparent, as shown in Fig. 5 (c), macroscopically revealing the transition, and only micelles of the order of tens of nanometers are found [4-6]. In addition, the Figure 5 (d) shows the evolution on the optical absorption of the set of samples at different temperatures. The absorption has been measured by the means of a UV/Vis spectrophotometer (JENWAY 6405 UV/Vis spectrophptometer). The data consist of three different spectra per sample, with each measurement taking 30 seconds to be acquired.

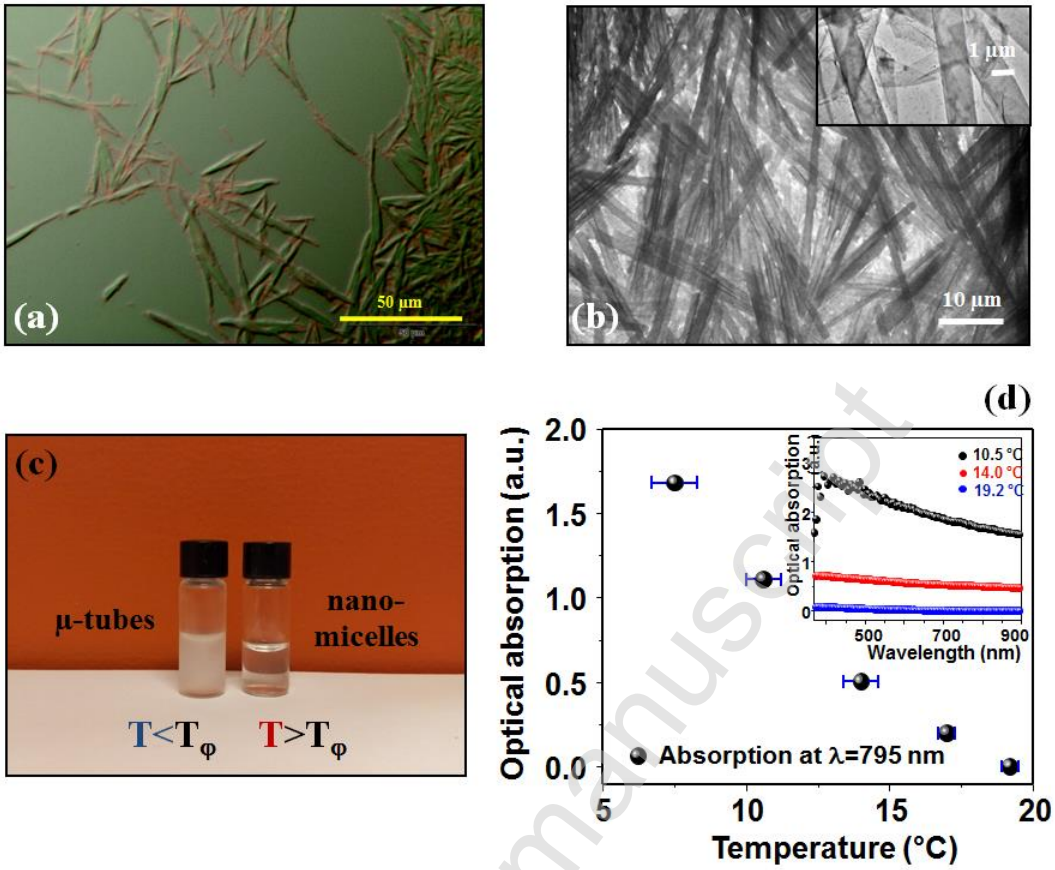

Fig. 5. Photographs of the C5/12-HSA compound, (a) at 7.5 °C. (b) Transmission electron microscopy (TEM) image of the multi-lamellar tubes (molar ratio R=0,3). Picture (c) represents the turbidity of the two states where for nano-micelles the liquid is transparent, while for tubes the solution is milky at a temperature below the transition temperature T_{φ}. Figure (d) shows the optical absorption properties the set of samples under different temperatures.

These absorption evolutions were measured at 795 nm, i.e. the working wavelength on the biophotonic sensor based on IO microresonators. Both a clear collapse on the absorbance intensity and a more transparent solution are observed as temperature increases; then above a critical temperature, the absorption contribution due to the presence of tubes is no longer observed by UV-vis spectroscopy measurements. Note lastly that the formed structures inside the C5/12-HSA solution at different temperatures reproduce well those obtained in previous work [6]. Also, the same reversibility with temperature is recovered, as in previous studies [4-6].

3.2 The main optical microcavity properties and their correlation with the thermoresponsive C5/12-HSA compound

By considering the thermo-photonic protocol exposed above, we highlight that the thermal properties of our IO device are ideal to monitor the thermo-responsivity of the C5/12-HSA system. The experiments were carried out from 17 to 24 °C with steps of 0.5 °C. The thermal evolution results are presented in Figure 6 (a, b) in terms of FSR and FWHM parameters of the IO device. The graphs Figure 6 (a) and (b) representing the evolution of the FSR (respectively of FWHM) are normalized with respect to the value of FSR (respectively FWHM) at the lowest considered temperature, namely 17°C. Additionally, the thermal dependency of these spectral parameters have been measured (Figure 6 (c) and (d)) for the bare sensor, and subtracted to the results obtained for the phase transition. Indeed, this way, the effects due to the measured phase transition can be discriminated from the intrinsic thermal drift of the bare photonic structure.

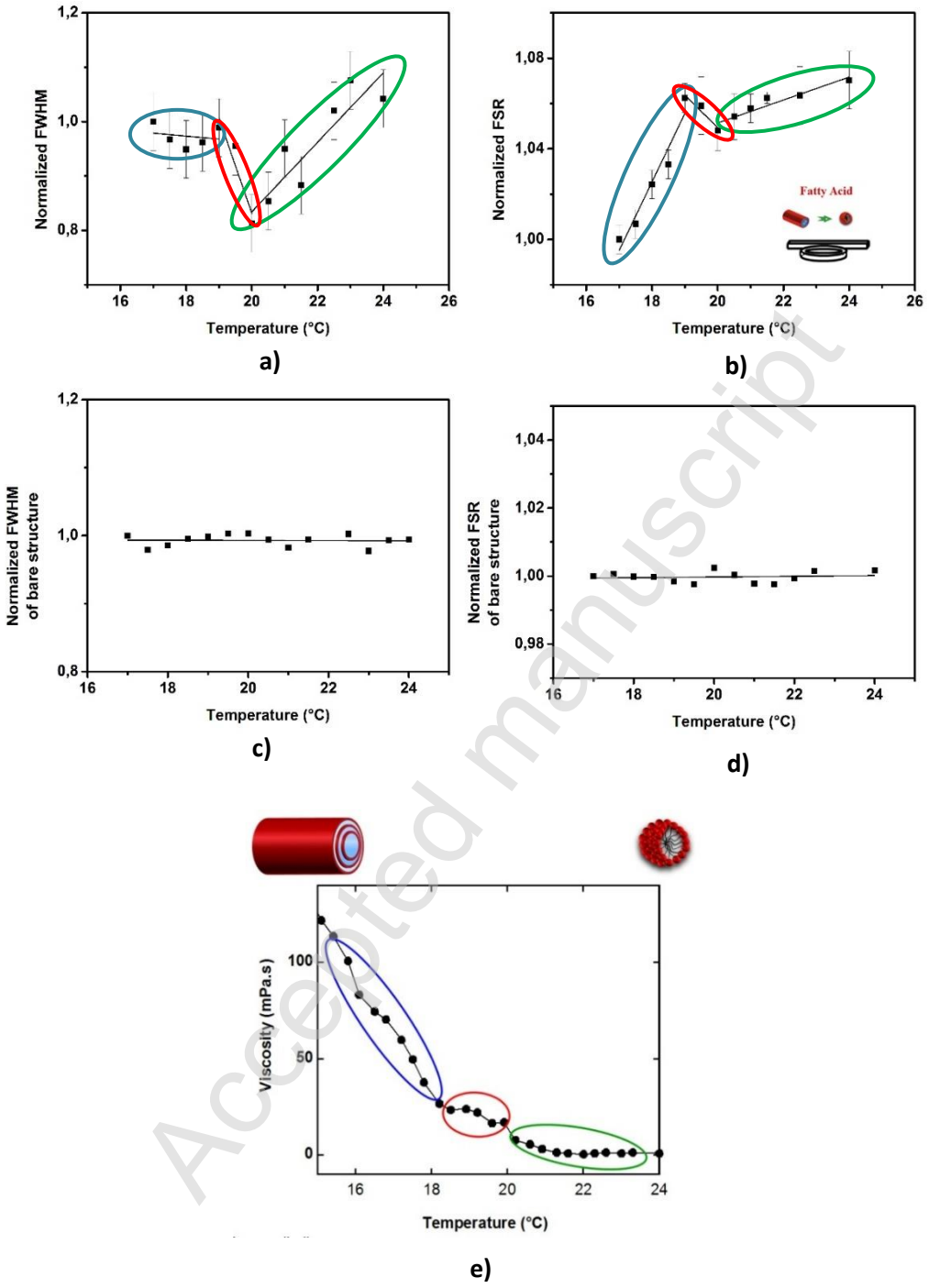

Fig. 6. Phase transition detection of the C5/12-HSA system base on the main optical properties of the IO device: (a) FWHM (b) FSR. Measurements were done from 17 to 24°C. A two –step transition ranging between 18.5 and 19.5°C is observable**.** (c) and (d) represent the thermal response of the bare structure concerning the FWHM and FSR respectively. (e) Study of the dynamic viscosity of the C5/12-HSA system evidencing different regimes, with an intermediate one between 18 and 20 ºC.

The processing of the transmission spectra were successfully achieved and demonstrate that the obtained values for the FSR and FWHM unambiguously depend on temperature: the thermo-responsivity of the solution is not only revealed by a single kink in these curves, but it turns out that three different regimes can be identified, as in Fig. 6(a) and 6(b). From 17 to 18.5 °C the thermo-responsive behavior is observed in the FSR evolution which increases, corresponding to a diminution of n_{eff}^{tot}, while the FWHM remains constant. As the FSR and the FWHM have the same dependency regarding $\frac{1}{n_{eff}^{tot}}$, we can deduce from the constant value of FWHM on the range [17°C ; 18,5°C] that the variation of the $arccos(\frac{2AK}{1+A^2K^2})$ factor in its expression compensates the variation of effective index. Then, in the range [18.5°C – 20°C], the slope of the FSR is inverted, i.e. the FSR value decreases (n_{eff}^{tot} increases), together with the FWHM. The diminution of both the FSR and the FWHM shows that, referring to their expressions, the contribution of the $\frac{1}{n_{eff}^{tot}}$ factor appears more important than the contribution of the $arccos(\frac{2AK}{1+A^2K^2})$ one; the main contribution to the changes of FWHM is the variation of the effective index, and not the variations of coupling and loss. Finally, the third regime (for T > 20°C) reveals another slope inversion for both the FWHM and the FSR. Once again, the fact that both the FSR and FWHM vary in the same direction shows that the change in effective index is more important that the change of coupling and loss conditions of the all structure. Indeed, below the phase transition temperature, the product is shaped as micro tubular with dimensions greater than the working wavelength, which causes scattering that modifies greatly the loss and coupling. In comparison, above this temperature, the micelles have a sub-wavelength dimension so that the solution acts as an effective medium regarding the optical mode propagating in the resonator, thus reducing the scattering to the point where it becomes negligible compared to the effective index variations.The quality factor as also been tracked as shown in Figure 7. This graph clearly exhibit the same characteristics as the graphs representing FSR and FWHM, i.e. two slope breaking at 18.5°C and 20°C, which is the signature of the phase transition. For the whole range of temperature, the quality factor has a value comprised between 200 and 300, which is not the maximal value obtainable with such a microresonator, but sufficient to detect the studied phase transition. At this stage, one has to compare these results to some other independent measurements of the structures inside the solution, in order to check if the optical results actually correspond to changes at the supramolecular scale. In that respect, a viscosity measurement of the solution was carried out using an Anton Paar rheometer (MCR 301) with a cone-plate setup: the shear rate was

fixed at $0.5s^{-1}$ and the temperature was slowly varied from 12 to 25°C. Indeed, the variation of the viscosity can be directly related to the changes of supramolecular structures inside the solution [6].

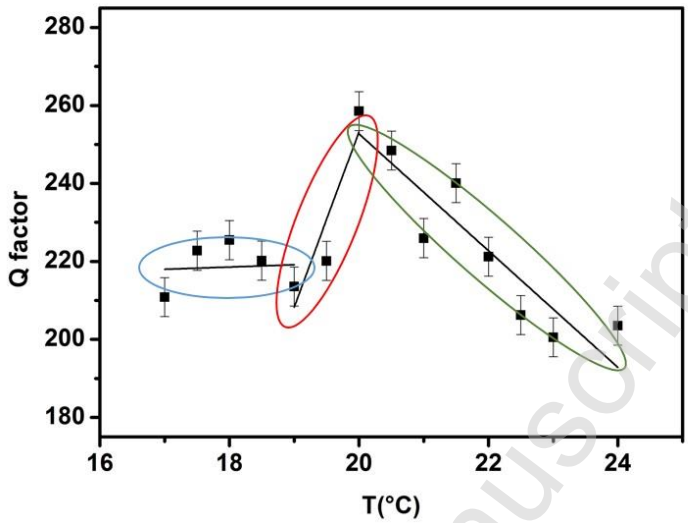

Fig.7. Evolution of the quality factor (Q) on the range [17°C; 24°C]. As in figure 6 (a) and (b), the phase transition is visible through the slope breaking at 18.5°C and 20°C.

The dynamic viscosity is shown in Figure 6 (e): the viscosity decreases by a factor ~100 as the temperature is varied from 16 to 24°C. Based on previous work [6] one can link this decrease to the tube-micelle transition. The low viscosity found for T > 20°C is indeed consistent with a micellar and Newtonian solution (green circle in Fig.6c). For T < 20°C - where the viscosity is high meaning that there are large structures in the solution - one can separate the curve in two parts (blue and red circles in Fig. 6c): an intermediate state can be identify between 18,5°C and 20°C, probably corresponding to intermediate structures between the tubes at low temperatures and the micelles at high temperatures. Note also that - quantitatively - this thermo-responsive behavior of the C5/HSA system (with micelles occurring above 20°C) is slightly different to the one reported in reference [6] (where micelles occurs for T > 23-25°C): this is simply due to the lower purity of the 12-HSA sample used here. It is actually expected that impurities slightly reduce the transition temperatures [4-6].

Finally, it turns out that these rheological results agree very well with those obtained by our hybrid IO device. The two techniques reveal the same three regimes and a transition occurring in two steps as T is varied, with an intermediate regime between 18,5°C and 20°C. Therefore, this validates the viability of the optical device to monitor supramolecular changes in such fluid solutions. During this morphological phase transition of fatty acids, the detections using resonant light probes are particularly interesting in terms of accuracy. Indeed, the rates of variation of both

the optical parameters FWHM(*T*) and FSR(*T*) change their signs as *T* is increased (Fig. 6 (a) and (b)), while the viscosity only evolve in a monotonous way. As a consequence, the three different regimes are much better identified with the optical tool, than with the rheological one.

4. Conclusion

This work reports the high versatility on the performance of an integrated optical polymeric micro-cavity, based on a resonance probe light, to carry out phase transition detection of self-assembled surfactant system used in cosmetic products, food and biology. The C5/12-HSA thermo-responsive behavior was monitored by the overall experimental protocol where a set of spectra were both statistically and originally presented by considering the FSR and FWHM main optical properties of the integrated device. The measurements showed that the temperature transition occurs in two steps, with an intermediate regime between 18,5C and 20°C. We show that these optical results can be directly related to the morphological changes of the surfactant passing from elongated self-assembled tubes to micelles. A complementary rheological study was done with the aim of validating this interpretation and corroborating the obtained transition temperatures. The studies demonstrated the high degree of accuracy with respect to the range of temperature where the transition occurs. The comparative study also showed that the IO device had a higher accuracy to reveal all the details of the transition, while the rheological probe hardly detects these changes. In conclusion, the proof of concept of the sensing platform which allowed continuous real time monitoring was fully demonstrated. The polymeric resonator together with the measurement protocol demonstrated high versatility in their performance to carry out investigations related with phase transition of novel thermo-responsive materials and food or cosmetic products presenting micro-structuration when outdated and expired with time.

Acknowledgments

The authors would like to thank the 'Direction de l'Innovation et des Relations avec les Entreprises'(DIRE) of the CNRS, Rennes Metropolis and Fondation Rennes 1 for financially supporting this research.

References

[1] A.-L. Fameau, F. Cousin, L. Navailles, F. Nallet, F. Boué, J.-P. Douliez, Multiscale Structural Characterizations of Fatty Acid Multilayered Tubes with a Temperature-Tunable Diameter, The Journal of Physical Chemistry B, 115 (2011) 9033-9039.

[2] C.V. Kulkarni, Lipid Self-Assemblies and Nanostructured Emulsions for Cosmetic Formulations, Cosmetics, 3 37 (2016) 1-15.

[3] C. Salerno, D.A. Chiappetta, A. Arechavala, S. Gorzalczany, S.L. Scioscia, C. Bregni, Lipid-based microtubes for topical delivery of Amphotericin B, Colloids and Surfaces B: Biointerfaces, 107 (2013) 160-166.

[4] J.-P. Douliez, B. Pontoire, C. Gaillard, Lipid Tubes with a Temperature-Tunable Diameter, ChemPhysChem, 7 (2006) 2071-2073.

[5] A.-L. Fameau, F. Cousin, L. Navailles, F. Nallet, F. Boué, J.-P. Douliez, Multiscale structural characterizations of fatty acid muiltilayered tubes with a temperature-tunable diameter, Journal of Physcial chemistry B, 115 (2011) 9033-9039.

[6] A.-L. Fameau, F. Cousin, A. Saint-Jalmes, Morphological Transition in Fatty Acid Self-Assemblies: A Process Driven by the Interplay between the Chain-Melting and Surface-Melting Process of the Hydrogen Bonds, Langmuir, 33 (2017) 12943-12951.

[7] A.-L. Fameau, A. Saint-Jalmes, F. Cousin, B. Houinsou Houssou, B. Novales, L. Navailles, F. Nallet, C. Gaillard, F. Boué, J.-P. Douliez, Smart Foams: Switching Reversibly between Ultrastable and Unstable Foams, Angewandte Chemie International Edition, 50 (2011) 8264-8269.

[8] A. Arnould, A.A. Perez, C. Gaillard, J.-P. Douliez, F. Cousin, L.G. Santiago, T. Zemb, M. Anton, A.-L. Fameau, Self-assembly of myristic acid in the presence of choline hydroxide: Effect of molar ratio and temperature, Journal of Colloid and Interface Science, 445 (2015) 285-293.

[9] N. Michel, A. S. Fabiano, A. Polidori, R. Jack, B. Pucci, Determination of phase transition temperatures of lipids by light scattering, Chem. Phys. Lipids, 139 11 (2006) 11-19.

[10] D.G. Rabus , Integrated ring resonators The compendium, Ed. 2007 Berlin: Springer.

[11] J. Scheuer, A. Yariv, Fabrication and characterization of low-loss polymeric waveguides and micro-resonators, J. Eur. Opt. Soc., 1 (2006) 06007.1-06007.5

[12] C. Delezoide, M. Salsac, J. Lautru, H. Leh, C. Nogues, J. Zyss, M. Buckle, I. Ledoux-Rak, C.T. Nguyen, Vertically Coupled Polymer Microracetrack Resonators for Label-Free Biochemical Sensors, IEEE Photonics Technology Letters, 24 (2012) 270-272.

[13] M.-Carmen Estevez, Mar Alvarez and Laura M. Lechuga, Integrated optical devices for

lab-on-a-chip biosensing applications, Laser Photonics Rev., 6 (2011) 1–25.

[14] R. Castro Beltran, N. Huby, V. Vié, H. Lhermite, L. Camberlein, E. Gaviot, B. Bêche, A laterally coupled UV210 polymer racetrack micro-resonator for thermal tunability and glucose sensing capability, Advanced Device Materials, 1 (2015) 80-87.

[15] H.K. Hunt, A.M. Armani, Label-free biological and chemical sensors, Nanoscale, 2 (2010) 1544-
1559.

[16] Q. Li, V. Vié, H. Lhermite, E. Gaviot, C. Bourlieu, A. Moréac, D. Morineau, D. Dupont, S. Beaufils, B. Bêche, Polymer resonators sensors for detection of sphingolipid gel/fluid phase transition and melting temperature measurement, Sensors and Actuators A: Physical, 263 (2017) 707-717.

[17] C.-Y. Chao, L.J. Guo, Biochemical sensors based on polymer microrings with sharp asymmetrical resonance, Applied Physics Letters, 83 (2003) 1527-1529.

[18] C. Chung-Yen, W. Fung, L.J. Guo, Polymer microring resonators for biochemical sensing applications, IEEE Journal of Selected Topics in Quantum Electronics, 12 (2006) 134-142.

[19] A.-L. Fameau, A. Arnould, A. Saint-Jalmes, Responsive self-assemblies based on fatty acidsCurrent Opinion in Colloid and Interface Science, 19 (2014) 471-479.

[20] Rohm and Haas Electronic Materials UVTM 210 Postitive DUV Photoresist, (2014) (http://www.microchem.com/Prod-DowElect-UV210GS.htm)

[21] D. Pluchon, N. Huby, H. Lhermite, D. Duval, B. Bêche, Investigation of fabrication and resonant optical coupling in various 2D micro-resonator structures in a UV210 polymer, Journal of Micromechanics and Microengineering, 22 (2012) 085016.1-085016.8

[22] R. Castro-Beltran, N. Huby, G. Loas, H. Lhermite, D. Pluchon, B. Bêche, Improvement of efficient coupling and optical resonances by using taper-waveguides coupled to cascade of UV210 polymer micro-resonators, Journal of Micromechanics and Microengineering, 24 (2014) 125006.1-125006.7.

[23] C.-Y. Chao, Polymer microring resonators for biochemical sensing applications, PhD Thesis, University of Michigan (2005).

[24] B. Bêche, J.F. Jouin, N. Grossard, E. Gaviot, E. Toussaere, J. Zyss, PC software for analysis of versatile integrated optical waveguides by polarized Semi-Vectorial Finite Difference Method, Sensors and Actuators : Physical A, 114/1 (2004) 59-64.

[25] L. Garnier, C. Saavedra, R. Castro-Beltrán, J. L. Lucio M., E. Gaviot, B. Bêche Hybrid composed method associating conformal transformation with matrix formulation for

computing eigenvalues and eigenvectors in bended optical waveguides, Optik 142 (2017) 536-540.

[26] M. Heiblum, J. H. Harris, Analysis of Curved Optical Waveguides by Conformal Transformation, IEEE JQE 11 (1975) 75-83.

[27] M. Lebental, Chaos quantique et micro-lasers organiques, PhD Thesis, University of Paris 11 ENS Cachan Paris-Sud, (2007).